Frequency Response Data-Driven Multi-Axis Add-On Structure Feedback Controller Design Applied to 3-DOF High-Precision Motion System

Masahiro Mae
The University of Tokyo
Tokyo 113-8656, Japan
mmae@ieee.org

Yi-Ping Hsin
Nikon Research Corporation of America
CA 94002-4107, U.S.A.
yiping.hsin@nikon.com

Koichi Sakata
Nikon Corporation
Tokyo 140-8601, Japan
koichi.sakata@nikon.com

***Abstract*—Feedback controller design for multivariable motion systems presents a challenge due to the numerous tuning parameters and complex coupling dynamics. The aim of this paper is to develop a data-driven design procedure for decentralized feedback controllers in multi-axis motion systems. The decentralized feedback controller in each axis is constructed in an add-on structure, and the parameters are designed by iterative convex optimization using frequency response data. The developed approach enables interpretability in the optimized feedback controllers due to their structured representation, and the coupling dynamics between each axis can be considered by the data-driven optimization. The performance improvement is validated through numerical simulation based on experimental data from a 3-DOF high-precision motion system.**

***Index Terms*—PID controller, Resonant filter, Loop shaping, MIMO system, Frequency response data, Convex optimization**

I. Introduction

In the feedback controller design of multi-input multi-output (MIMO) motion systems, frequency response data-driven optimization has the advantage of tuning numerous parameters, compared to single-input single-output (SISO) motion systems with fewer tuning parameters. For the interpretability of the feedback controller, the structured feedback controller design via convex optimization using frequency response data is developed, such as the Proportional-Integral-Derivative (PID) controller [1] that can be extended to the MIMO system [2], [3], [4], and peak filter [5] that is successfully implemented to the industrial MIMO motion system with complex coupling dynamics. In the structured feedback controller design, the resonant filter can cope with the disturbance at the specific frequency [6], and that is also successfully applied to the industrial MIMO motion system [7].

To balance the trade-off of the performance enhancement with several feedback controllers, the controllers should be designed simultaneously, such as a P-PI controller and a self resonance cancellation [8], a PID controller and an all-pass filter [9], in addition to a notch filter [10], but the optimization becomes nonlinear and non-convex. The linear parameterization enables the convex optimization of feedback controllers, which is successfully applied in notch and peak filters [11], and stable and unstable resonant filters [12].

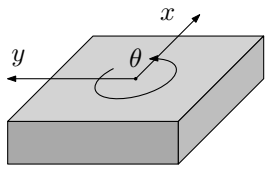

Fig. 1. Schematic illustration of the 3-DOF motion system.

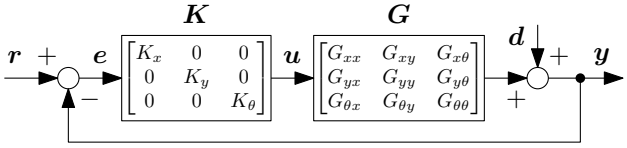

Fig. 2. Block diagram of the 3-DOF decentralized controlled system.

Although several approaches have been developed for the structured feedback controller design using frequency response data, the trade-off of the disturbance rejection performance between the low and specific frequencies is not explicitly taken into account. In this paper, the developed approach provides the simultaneous design of the PID controller for the fundamental disturbance rejection performance at the low frequency and the resonant filters for the enhanced disturbance rejection performance at the specific frequency.

The main contributions of this paper are as follows.

(C1) Feedback controllers for low and specific frequency disturbances are designed simultaneously to maximize the disturbance rejection performance.

(C2) Feedback controllers are designed by iterative convex optimization using frequency response data of a multi-axis motion system.

II. Problem formulation

Fig. 1 shows the schematic illustration of the 3-DOF high-precision motion system with (x, y, θ)-axes. Fig. 2 shows the 3-DOF decentralized controlled system. In this paper, the decentralized feedback controller $\boldsymbol{K}$ is designed for the MIMO controlled system $\boldsymbol{G}$ to reject the output disturbance

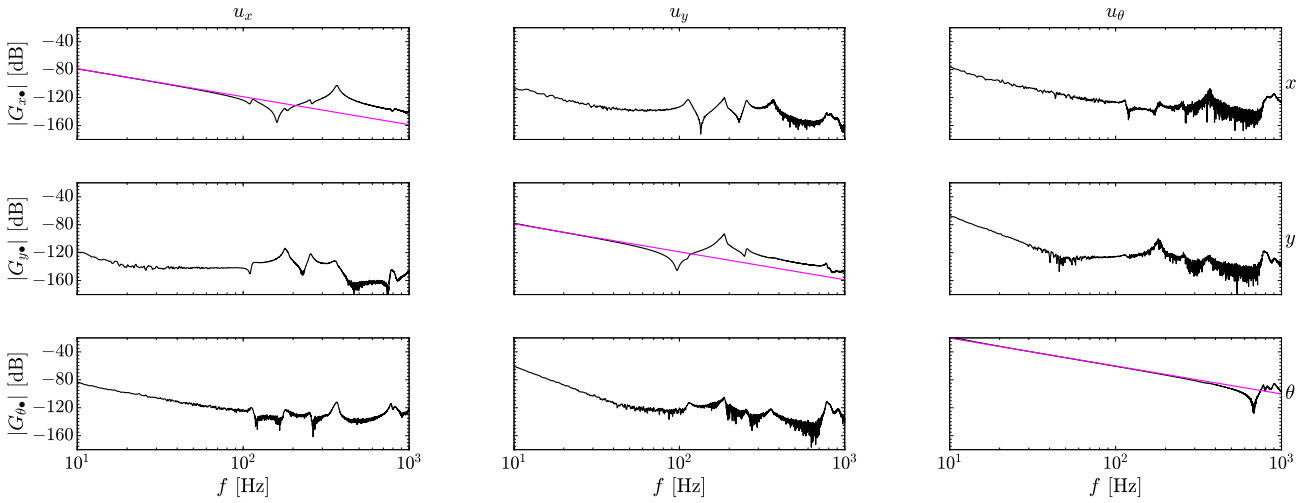

Fig. 3. Bode magnitude plot of frequency response in the 3-DOF experimental setup. Frequency response data $\boldsymbol{G}(\mathrm{j}\omega_{k_f})$ is shown in (—) and the diagonal rigid body model $\boldsymbol{G}_d(s)$ is shown in (—).

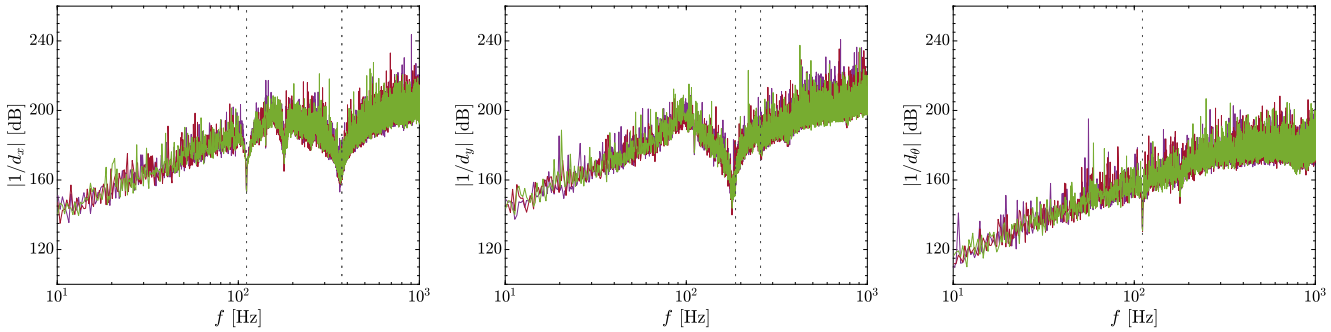

(a) x (b) y (c) θ

Fig. 4. Inverse disturbance spectrum. Vertical black dotted lines (---) correspond to resonance frequencies of designed resonant filters.

d. The Bode magnitude plot of the 3-DOF experimental setup is shown in Fig. 3. The inverse disturbance spectrum is shown in Fig. 4, which is obtained by the error frequency spectrum in the pre-experiment multiplied by the inverse of the sensitivity function matrix. The problem addressed in this paper is the decentralized multi-axis feedback controller design with respect to the following requirements.

(R1) Feedback controllers for low and specific frequency disturbances should be designed simultaneously to balance the trade-off of the Bode sensitivity integral.

(R2) Numerous tuning parameters of feedback controllers in a multi-axis motion system should be designed by convex optimization.

III. Frequency Response Data-Driven Multi-Axis Add-On Structure Feedback Controller Design

A. Definition of add-on structure feedback controller

For the decentralized feedback controller design in the MIMO system, the add-on structure feedback controller in each axis is shown in Fig. 5 and is defined as

$$
\begin{aligned}
K_{k_y}(\mathrm{j}\omega_{k_f}, \boldsymbol{\rho}_{k_y}) &= \rho_{k_y,p} + \frac{\rho_{k_y,i}}{(\mathrm{j}\omega_{k_f})} + \frac{\rho_{k_y,d}(\mathrm{j}\omega_{k_f})}{\tau_{k_y,d}(\mathrm{j}\omega_{k_f})+1} \\
&+ \sum_{k_r=1}^{n_{r,k_y}} \frac{\rho_{k_y,(k_r,2)}(\mathrm{j}\omega_{k_f})^2 + \rho_{k_y,(k_r,1)}(\mathrm{j}\omega_{k_f})}{(\mathrm{j}\omega_{k_f})^2 + 2\zeta_{r,k_y,k_r}\omega_{r,k_y,k_r}(\mathrm{j}\omega_{k_f}) + \omega^2_{r,k_y,k_r}} \\
&= \begin{bmatrix} \rho_{k_y,p} \\ \rho_{k_y,i} \\ \rho_{k_y,d} \\ \rho_{k_y,(1,1)} \\ \rho_{k_y,(1,2)} \\ \vdots \\ \rho_{k_y,(n_{r,k_y},1)} \\ \rho_{k_y,(n_{r,k_y},2)} \end{bmatrix}^{\mathsf{T}} \begin{bmatrix} 1 \\ \frac{1}{(\mathrm{j}\omega_{k_f})} \\ \frac{(\mathrm{j}\omega_{k_f})}{\tau_{k_y,d}(\mathrm{j}\omega_{k_f})+1} \\ \frac{(\mathrm{j}\omega_{k_f})}{(\mathrm{j}\omega_{k_f})^2+2\zeta_{r,k_y,1}\omega_{r,k_y,1}(\mathrm{j}\omega_{k_f})+\omega^2_{r,k_y,1}} \\ \frac{(\mathrm{j}\omega_{k_f})^2}{(\mathrm{j}\omega_{k_f})^2+2\zeta_{r,k_y,1}\omega_{r,k_y,1}(\mathrm{j}\omega_{k_f})+\omega^2_{r,k_y,1}} \\ \vdots \\ \frac{(\mathrm{j}\omega_{k_f})}{(\mathrm{j}\omega_{k_f})^2+2\zeta_{r,k_y,n_{r,k_y}}\omega_{r,k_y,n_{r,k_y}}(\mathrm{j}\omega_{k_f})+\omega^2_{r,k_y,n_{r,k_y}}} \\ \frac{(\mathrm{j}\omega_{k_f})^2}{(\mathrm{j}\omega_{k_f})^2+2\zeta_{r,k_y,n_{r,k_y}}\omega_{r,k_y,n_{r,k_y}}(\mathrm{j}\omega_{k_f})+\omega^2_{r,k_y,n_{r,k_y}}} \end{bmatrix} \\
&= \boldsymbol{\rho}_{k_y}^{\mathsf{T}} \boldsymbol{\phi}_{k_y}(\mathrm{j}\omega_{k_f}), \qquad (1)
\end{aligned}
$$

where the proportional, integral, and derivative gains are $\rho_{k_y,p}$, $\rho_{k_y,i}$, and $\rho_{k_y,d}$. The number of the resonant filters

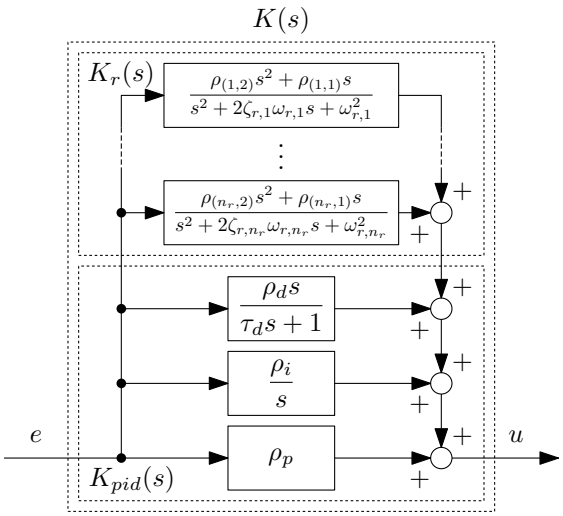

Fig. 5. Block diagram of add-on structure feedback controllers in each axis.

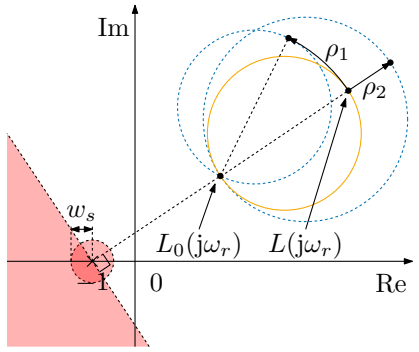

Fig. 6. Vector locus with resonant filter and robust stability condition.

in each axis is n_{r,k_y} and the index of the resonant filters is $k_r = 1, \ldots, n_{r,k_y}$. The phase, gain, resonance angular frequency, and damping coefficient of the resonant filters in each axis are $\rho_{k_y,(k_r,1)}$, $\rho_{k_y,(k_r,2)}$, ω_{r,k_y,k_r}, and ζ_{r,k_y,k_r}. The index of frequency response data is $k_f = 1, \ldots, n_f$. The tuning parameters are defined as $\boldsymbol{\rho}_{k_y} \in \mathbb{R}^{3+2n_{r,k_y}}$. The linear representation of the tuning parameters $\boldsymbol{\rho}$ and the basis functions $\boldsymbol{\phi}$ enables the iterative convex optimization using sequential linearlization with the frequency response data. The add-on structure has an advantage in the flexibility to accommodate the disturbance characteristics and the interpretability of the designed feedback controller for industrial applications.

B. Frequency response data-driven performance evaluation

The frequency response data of the controlled system is defined as

$$\boldsymbol{G}(\mathrm{j}\omega_{k_f}) = G_{(k_y,k_u)}(\mathrm{j}\omega_{k_f}), \tag{2}$$

where $k_u, k_y \in \{x, y, \theta\}$ are the indices of inputs and outputs, and the numbers of the input and the output are $n_u = n_y = 3$.

The element of the disturbance frequency spectrum matrix is defined as

$$\boldsymbol{D}(\mathrm{j}\omega_{k_f}) = \begin{bmatrix} \boldsymbol{d}_1(\mathrm{j}\omega_{k_f}) & \cdots & \boldsymbol{d}_{n_d}(\mathrm{j}\omega_{k_f}) \end{bmatrix}, \tag{3}$$

where the disturbance frequency spectrum in each column $\boldsymbol{d}_{k_d}(\mathrm{j}\omega_{k_f}) \in \mathbb{C}^{n_y \times 1}$ is defined as

$$\boldsymbol{d}_{k_d}(\mathrm{j}\omega_{k_f}) = \begin{bmatrix} d_{k_d,1}(\mathrm{j}\omega_{k_f}) & \cdots & d_{k_d,n_y}(\mathrm{j}\omega_{k_f}) \end{bmatrix}^{\mathsf{T}}, \tag{4}$$

where the number of the disturbance frequency spectrum is set to the same as the number of the input and the output of the controlled system for the matrix inverse calculation, as $n_u = n_y = n_d$. The error frequency spectrum matrix with the designed feedback controller is given by

$$\boldsymbol{E}(\mathrm{j}\omega_{k_f}, \boldsymbol{\rho}) = \boldsymbol{S}(\mathrm{j}\omega_{k_f}, \boldsymbol{\rho})\boldsymbol{D}(\mathrm{j}\omega_{k_f}), \tag{5}$$

where the sensitivity function matrix is $\boldsymbol{S}(\mathrm{j}\omega_{k_f}, \boldsymbol{\rho}) = (\boldsymbol{I} + \boldsymbol{G}(\mathrm{j}\omega_{k_f})\boldsymbol{K}(\mathrm{j}\omega_{k_f}, \boldsymbol{\rho}))^{-1} \in \mathbb{C}^{n_y \times n_y}$ with the designed feedback controller $\boldsymbol{K}(\mathrm{j}\omega_{k_f}, \boldsymbol{\rho})$. In MIMO systems, the unit of each output is different in several industrial applications, such as translation and rotation. Therefore, the normalized error frequency spectrum matrix is given by

$$\boldsymbol{W}^{-1}\boldsymbol{E}(\mathrm{j}\omega_{k_f}, \boldsymbol{\rho}) = \boldsymbol{W}^{-1}(\boldsymbol{I} + \boldsymbol{G}(\mathrm{j}\omega_{k_f})\boldsymbol{K}(\mathrm{j}\omega_{k_f}, \boldsymbol{\rho}))^{-1}\boldsymbol{D}(\mathrm{j}\omega_{k_f}), \tag{6}$$

where the scaling matrix is $\boldsymbol{W} \in \mathbb{R}^{n_y \times n_y}$.

When $n_u = n_y = n_d$, the inverse of the normalized error frequency spectrum matrix is given by

$$\boldsymbol{E}^{-1}(\mathrm{j}\omega_{k_f}, \boldsymbol{\rho})\boldsymbol{W} = \boldsymbol{D}^{-1}(\mathrm{j}\omega_{k_f})(\boldsymbol{I} + \boldsymbol{G}(\mathrm{j}\omega_{k_f})\boldsymbol{K}(\mathrm{j}\omega_{k_f}, \boldsymbol{\rho}))\boldsymbol{W}. \tag{7}$$

The performance is evaluated as the minimum square Frobenius norm of the normalized inverse error frequency spectrum matrix at each frequency, and the objective function is given by

$$\underset{\boldsymbol{\rho}}{\text{maximize}} \quad \min_{\forall k_f} \|\boldsymbol{D}^{-1}(\mathrm{j}\omega_{k_f})(\boldsymbol{I} + \boldsymbol{G}(\mathrm{j}\omega_{k_f})\boldsymbol{K}(\mathrm{j}\omega_{k_f}, \boldsymbol{\rho}))\boldsymbol{W}\|_F^2. \tag{8}$$

From the characteristics of the Frobenius norm and the singular value, the objective function becomes the sum of the inverse square singular value of the normalized error frequency spectrum matrix. In this formulation, the linear parameterization of the tuning parameters and the basis functions is maintained, which enables the iterative convex optimization using sequential linearlization.

C. Constraints of robust stability condition

In this paper, the robust stability condition consists of the gain and phase stability conditions, as shown in Fig. 6. The gain stability condition is defined as

$$|w_{s,k_y}(\mathrm{j}\omega_{k_f})| - \left|1 + G_{(k_y,k_y)}(\mathrm{j}\omega_{k_f})K_{k_y}(\mathrm{j}\omega_{k_f}, \boldsymbol{\rho})\right| \leq 0, \tag{9}$$

where the weighting function of the upper bound gain in the sensitivity function is $w_{s,k_y}(\mathrm{j}\omega_{k_f})$. Although the constraint of the sensitivity function is commonly used in the feedback controller design using frequency response data, the stability cannot be guaranteed only with the gain stability condition in the use of a controller that changes the gain and phase

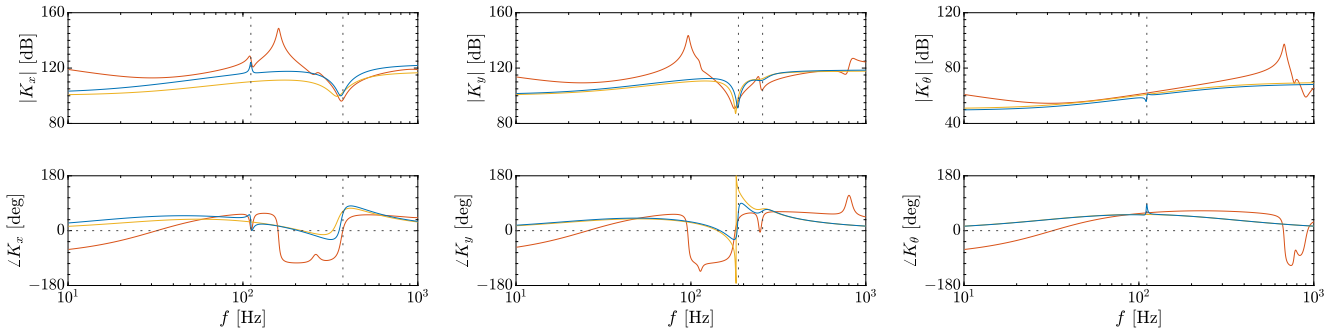

(a) x (b) y (c) θ

Fig. 7. Bode diagram of example (—), initial (—), and optimized (—) controllers. Vertical black dotted lines (---) correspond to resonance frequencies of designed resonant filters.

TABLE I
PARAMETERS IN DENOMINATORS OF RESONANT FILTERS.

	x_1	x_2	y_1	y_2	θ_1
ω_r	$2\pi \times 111$	$2\pi \times 373$	$2\pi \times 187$	$2\pi \times 257$	$2\pi \times 111$
ζ_r	0.01	0.5	0.2	0.15	0.01

with resonant modes, and the phase stability condition is introduced. The phase stability condition is defined as

$$-\frac{\pi}{2} \leq \angle\left(1 + G_{(k_y,k_y)}(\mathrm{j}\omega_{k_f}) K_{k_y}(\mathrm{j}\omega_{k_f}, \boldsymbol{\rho})\right) - \angle\left(1 + G_{d,k_y}(\mathrm{j}\omega_{k_f}) K_{0,k_y}(\mathrm{j}\omega_{k_f})\right) \leq \frac{\pi}{2}, \quad (10)$$

where G_{d,k_y} is the diagonal rigid body model and K_{0,k_y} is the initial diagonal PID controller. The phase stability condition represents that the vector locus with the optimized feedback controller is between the angle $\pm 90°$ of the angle from the origin of $(-1, \mathrm{j}0)$ to the normalized characteristics with the rigid body model and the PID controller. By integrating the gain and phase stabilization conditions, the vector locus with the optimized feedback controller must be on the same side as that of the normalized ones against $(-1, \mathrm{j}0)$ and outside of the modulus margin.

D. Optimization problem formulation

The optimization problem is formulated as

$$\underset{\boldsymbol{\rho}}{\text{maximize}} \quad \gamma \quad (11a)$$

$$\underset{\forall k_f, \forall, k_y}{\text{subject to}} \quad \gamma - \|\boldsymbol{D}^{-1}(\mathrm{j}\omega_{k_f})(\boldsymbol{I} + \boldsymbol{G}(\mathrm{j}\omega_{k_f})\boldsymbol{K}(\mathrm{j}\omega_{k_f}, \boldsymbol{\rho}))\boldsymbol{W}\|_F^2 \leq 0 \quad (11b)$$

$$|w_{s,k_y}(\mathrm{j}\omega_{k_f})| - \left|1 + G_{(k_y,k_y)}(\mathrm{j}\omega_{k_f}) K_{k_y}(\mathrm{j}\omega_{k_f}, \boldsymbol{\rho})\right| \leq 0 \quad (11c)$$

$$-\frac{\pi}{2} \leq \angle\left(1 + G_{(k_y,k_y)}(\mathrm{j}\omega_{k_f}) K_{k_y}(\mathrm{j}\omega_{k_f}, \boldsymbol{\rho})\right) - \angle\left(1 + G_{d,k_y}(\mathrm{j}\omega_{k_f}) K_{0,k_y}(\mathrm{j}\omega_{k_f})\right) \leq \frac{\pi}{2}, \quad (11d)$$

where the objective function is defined in the constraint with the parameter $\gamma \in \mathbb{R}_0^+$ of the objective function. The optimization problem can be solved by iterative convex optimization using sequential linearization [7].

IV. NUMERICAL SIMULATION IN 3-DOF MOTION SYSTEM

A. Condition

The number of frequency response data points is $n_f = 3245$, and the data points are arranged at linearly even intervals in the range from $10\,\mathrm{Hz}$ to $1000\,\mathrm{Hz}$. The frequency response data of the 3-DOF experimental setup $\boldsymbol{G}(\mathrm{j}\omega_{k_f})$ is shown in Fig. 3. The frequency response data of the inverse disturbance spectrum is shown in Fig. 4.

The Bode diagrams of the example and initial feedback controllers are designed heuristically as shown in Fig. 7. In the example feedback controller, the notch and peak filters are designed to cancel out the resonance and antiresonance of the diagonal terms, and the PID controller is designed by the pole placement method for the diagonal rigid body model.

In the initial feedback controller, the PD controllers are designed by the pole placement method for the diagonal rigid body model. Note that the integral gain of the initial feedback controller is $\rho_i = 0$ in each axis because of the PD controller structure, but the ρ_i can have a value in the optimized feedback controller through optimization. In the optimized feedback controllers, the time constants of the derivative controllers τ_d are set to the same as those of the initial ones.

In the initial feedback controller, the resonant filters are designed only for the stabilization of the resonant modes in the diagonal terms, and the gains of other resonant filters are set to 0. The resonance angular frequency ω_r and damping coefficients of the resonant filters are pre-defined as TABLE I from the shape of the disturbance spectrum.

In the robust stability condition, the modulus margin is set to $1/w_s = 6\,\mathrm{dB}$. The scaling matrix $\boldsymbol{W}$ is designed as a diagonal matrix with the root mean square error for each axis in the pre-experiment with the example controller. The iterative calculation in the optimization is continued until the improvement of the objective function is less than $0.1\,\%$. The optimization problem is computed in several minutes by the laptop with YALMIP [13] MOSEK [14] in MATLAB R2024b.

B. Optimization result

The Bode diagrams of the optimized feedback controllers are shown in Fig. 7. The Bode magnitude plots of the diagonal SISO sensitivity functions with example, initial, and optimized controllers are shown in Fig. 8. It shows that the feedback gains at the low frequency with the optimized controller become higher compared to those with the initial controllers. Both the PID controllers and the resonant filters are optimized

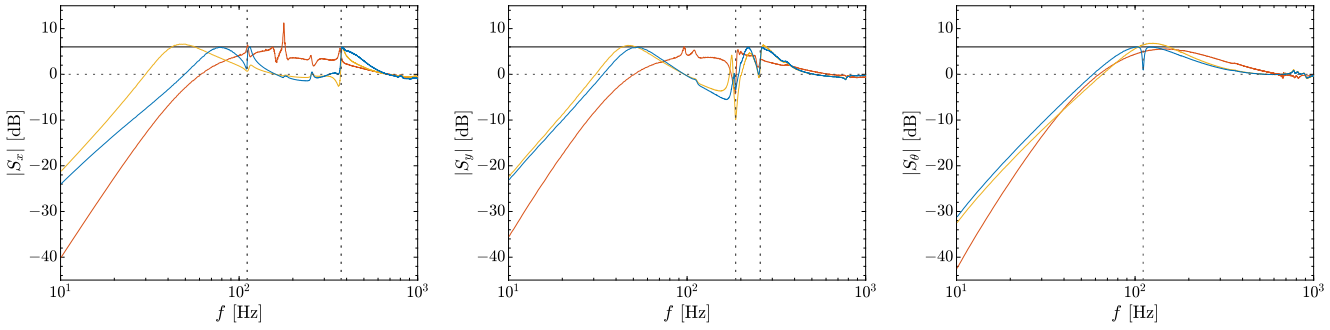

(a) x (b) y (c) θ

Fig. 8. Bode magnitude plot of SISO sensitivity functions with example (—), initial (—), and optimized (—) controllers. Constraints of 6 dB sensitivity peaks are shown as horizontal black solid lines (—). Vertical black dotted lines (---) correspond to resonance frequencies of designed resonant filters.

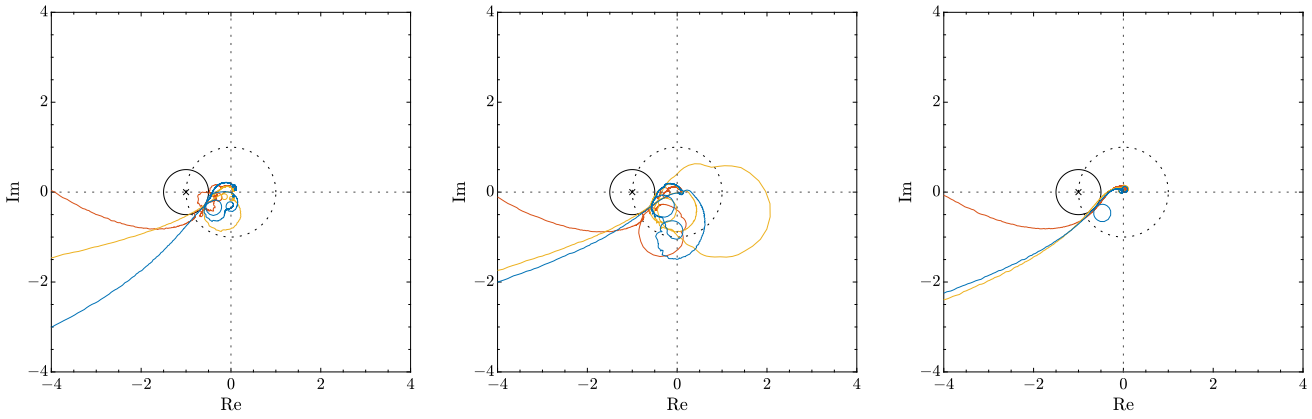

(a) x (b) y (c) θ

Fig. 9. Nyquist diagram with example (—), initial (—), and optimized (—) controllers. 6 dB modulus margins are shown as black solid circles (—).

simultaneously as the sensitivity functions follow the shape of the inverse disturbance spectrum to improve the disturbance rejection performance.

Nyquist diagrams of the diagonal SISO open-loop systems with example, initial, and optimized controllers are shown in Fig. 9. It shows that the optimized controllers satisfy the robust stability conditions, which are not satisfied by the example and initial ones.

C. Performance evaluation

After the optimization, the eigenvalue loci are used for the analysis of the necessary and sufficient stability condition in MIMO systems. Fig. 10 shows the eigenvalue loci with example, initial, and optimized controllers. It shows that the eigenvalue loci in the example controller have several changes from the SISO Nyquist diagram because of the coupling dynamics between each axis. In contrast, the eigenvalue loci in the initial and optimized controllers are consistent because of the phase stabilization of the mechanical resonant modes that reduces the coupling effects between each axis.

For the MIMO performance evaluation, the cumulative amplitude spectrum errors in each axis are shown in Fig. 11. It shows that disturbance rejection performance is improved at the frequencies with resonant filters, and the total performance is balanced with the trade-off to the disturbance rejection performance in the low frequency. From the identity of Parseval's theorem between the time domain signal and the frequency domain signal in the square integral, the cumulative amplitude spectrum errors are identical to the root mean square errors in the time domain error signals. From that identity, the root mean square errors in each axis are improved by the optimized feedback controllers in all (x, y, θ)-axes compared to the example and initial ones.

V. Conclusion

Feedback controller design for multivariable motion systems presents a challenge due to the numerous tuning parameters and complex coupling dynamics. In this paper, a data-driven design procedure for decentralized feedback controllers in multi-axis motion systems is developed. The decentralized feedback controller in each axis is constructed in an add-on structure that enables interpretability in the optimized feedback controllers. The parameters are designed by frequency response data-driven iterative convex optimization for considering the coupling dynamics between each axis. The performance improvement is validated through numerical

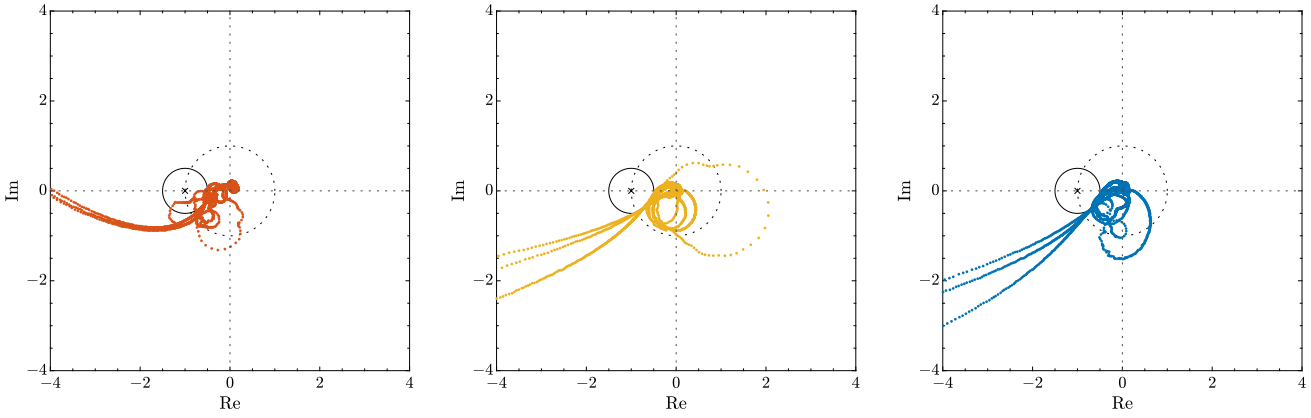

(a) example (b) initial (c) optimized

Fig. 10. Eigenvalue loci with example (—), initial (—), and optimized (—) controllers. 6 dB modulus margins are shown as black solid circles (—).

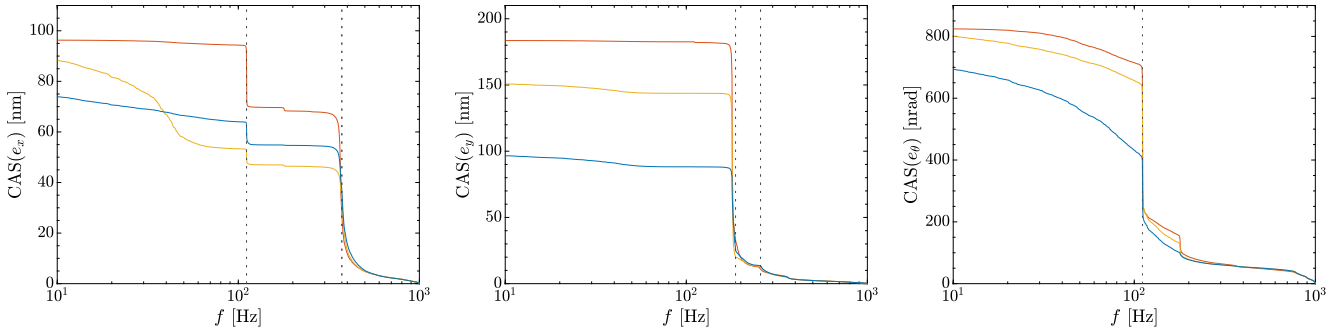

(a) x (b) y (c) θ

Fig. 11. Cumulative Amplitude Spectrum (CAS) errors from high to low frequency with example (—), initial (—), and optimized (—) controllers. Vertical black dotted lines (---) correspond to resonance frequencies of designed resonant filters.

simulation based on experimental data from a 3-DOF high-precision motion system. Ongoing research focuses on the nonlinear optimization with the coefficients in the denominator of the feedback controller and the practical design procedure of the initial parameter in closed-loop stable conditions.

REFERENCES

[1] A. Karimi and G. Galdos, "Fixed-order H_∞ controller design for nonparametric models by convex optimization," *Automatica: the journal of IFAC, the International Federation of Automatic Control*, vol. 46, no. 8, pp. 1388–1394, 2010.

[2] S. Boyd, M. Hast, and K. J. Åström, "MIMO PID tuning via iterated LMI restriction," *International Journal of Robust and Nonlinear Control*, vol. 26, no. 8, pp. 1718–1731, 2016.

[3] S. Shinoda, K. Yubai, D. Yashiro, and J. Hirai, "Multivariable Controller Design Achieving Diagonal Dominance Using Frequency Response Data," *Electronics and Communications in Japan*, vol. 100, no. 10, pp. 12–23, 2017.

[4] P. Schuchert, V. Gupta, and A. Karimi, "Data-driven fixed-structure frequency-based H_2 and H_∞ controller design," *Automatica*, vol. 160, no. 111398, p. 111398, 2024.

[5] M. Mae, W. Ohnishi, H. Fujimoto, K. Sakata, and A. Hara, "Frequency response data-based peak filter design applied to MIMO large-scale high-precision scan stage," *Mechatronics*, vol. 83, no. 102733, p. 102733, 2022.

[6] M. Mae, W. Ohnishi, and H. Fujimoto, "Frequency Response Data-based Resonant Filter Design considering Phase Stabilization and Stroke Limitation applied to Dual-Stage Actuator Hard Disk Drives," in *The 22nd IFAC World Congress*, vol. 56, 2023, pp. 10 614–10 619.

[7] M. Mae, W. Ohnishi, H. Fujimoto, and K. Sakata, "Multi-Axis Resonant Filter Design using Frequency Response Data applied to Industrial Scan Stage," *IEEE/ASME Transactions on Mechatronics*, vol. 29, no. 4, pp. 2867–2876, 2024.

[8] W. Ohnishi, "Data-based feedback controller tuning utilizing collocated and non-collocated sensors," in *The 8th IFAC Symposium on Mechatronic Systems*, vol. 52, 2019, pp. 157–162.

[9] E. Kuroda, Y. Maeda, and M. Iwasaki, "Efficient Autonomous Design of Cascade Structure Feedback Controller Parameters Realizing Robust Stabilization," *IEEJ Journal of Industry Applications*, vol. 13, no. 1, pp. 34–40, 2024.

[10] T. Shiohara and Y. Maeda, "Enhanced Auto-Tuning of Feedback Controllers with Aggressive Search Ensuring Stability and Its Application to Galvano Scanner," *IEEJ Journal of Industry Applications*, vol. 13, no. 5, pp. 539–546, 2024.

[11] M. Mae, "Data-Driven Multiple Resonant Filter Design Integrating Notch Filters and Peak Filters in Dual-Stage Actuator Hard Disk Drives," in *2025 IEEE International Conference on Mechatronics (ICM)*. IEEE, 2025, pp. 1–6.

[12] M. Mae, "Data-Driven Loop-Shaping with Resonant Filters Integrating Unstable and Stable Poles in Dual-Stage Actuator Hard Disk Drives," in *The 10th IFAC Symposium on Mechatronic Systems*, 2025.

[13] J. Lofberg, "YALMIP : a toolbox for modeling and optimization in MATLAB," in *2004 IEEE International Conference on Robotics and Automation*. IEEE, 2004, pp. 284–289.

[14] MOSEK ApS, "MOSEK Optimization Toolbox for MATLAB Version 10.2," https://docs.mosek.com/10.2/toolbox/index.html, 2024.